
This is an electronic reprint of the original article.
This reprint may differ from the original in pagination and typographic detail.

Shahzad, S.; Niiranen, J.

Analytical solution with validity analysis for an elliptical void and a rigid inclusion under uniform or nonuniform anti-plane loading

Published in:
Theoretical and Applied Fracture Mechanics

DOI:
[10.1016/j.tafmec.2018.07.009](https://doi.org/10.1016/j.tafmec.2018.07.009)

Published: 01/10/2018

Document Version
Peer-reviewed accepted author manuscript, also known as Final accepted manuscript or Post-print

Published under the following license:
CC BY-NC-ND

Please cite the original version:
Shahzad, S., & Niiranen, J. (2018). Analytical solution with validity analysis for an elliptical void and a rigid inclusion under uniform or nonuniform anti-plane loading. *Theoretical and Applied Fracture Mechanics*, 97, 62-72. <https://doi.org/10.1016/j.tafmec.2018.07.009>

This material is protected by copyright and other intellectual property rights, and duplication or sale of all or part of any of the repository collections is not permitted, except that material may be duplicated by you for your research use or educational purposes in electronic or print form. You must obtain permission for any other use. Electronic or print copies may not be offered, whether for sale or otherwise to anyone who is not an authorised user.

See discussions, stats, and author profiles for this publication at: <https://www.researchgate.net/publication/326606271>

Analytical solution with validity analysis for an elliptical void and a rigid inclusion under uniform or nonuniform anti-plane loading

Article in *Theoretical and Applied Fracture Mechanics* · July 2018

DOI: 10.1016/j.tafmec.2018.07.009

CITATIONS

0

READS

10

2 authors:



Summer Shahzad

Ramboll, Espoo, Finland

10 PUBLICATIONS **43** CITATIONS

[SEE PROFILE](#)



Jarkko Niiranen

Aalto University

44 PUBLICATIONS **264** CITATIONS

[SEE PROFILE](#)

Some of the authors of this publication are also working on these related projects:



Accademia [View project](#)



Models and methods for mechanics of solids and structures -- strain gradient continuum theories with computational analysis [View project](#)

Analytical solution with validity analysis for an elliptical void and a rigid inclusion under uniform or nonuniform anti-plane loading

S. Shahzad¹ and J. Niiranen^{1,2}

¹Department of Civil Engineering, Aalto University,
Rakentajanaukio 4, 02150 Espoo, Finland, Finland

² Faculty of Civil Engineering and Geodesy, Technische Universität
München, Arcisstr. 21, 80333 München, Germany

Abstract

An elliptical inclusion (covering both void and rigid inclusions) embedded in an infinite and finite elastic plane subject to uniform and nonuniform (m-th order polynomial) anti-plane loading conditions is analyzed. An analytical solution in terms of the stress field for an infinite plane is developed through the method of analytic function and conformal mapping. Closed-form complex potentials and analytical expressions for Stress Concentration Factors (SCFs) are obtained. The results show that (i.) the SCF value decreases with an increasing loading order, so that the influence of the non-uniformity of the anti-plane loads on the SCF is revealed to be beneficial from the failure point of view; (ii.) decrease in the SCF value for an infinite plane is monotonic, which does not hold true for a finite plane. The results for an infinite plane are confirmed and extended for finite planes by exploiting the well-known heat–stress analogy and the finite element method. It is worth mentioning that the comparison between the analytical solution for an infinite plane and the numerical solution for finite plane is provided, showing that the analytical solution of an infinite plane can be used as an accurate approximation to the case of a finite plane. Moreover, the proposed heat–stress analogy can be exploited to study the crack–inclusion interaction or multiply connected bodies. The computational efficiency of the proposed methodology makes it an attractive analysis tool for anti-plane problems with respect to the full scale three-dimensional analysis.

Keywords: anti-plane elasticity, SCF, SIF, crack, heat–stress analogy, composites, Laplace equation.

1 Introduction

The increasing demand of lightweight high-strength composite materials is undeniable in a wide range of applied sciences such as structural, mechanical, aerospace, nuclear and

chemical engineering. On the other hand, voids, cracks, defects and inclusions in structures are known to generate stress concentrations and they are detrimental to the overall strength and durability of structure. For instance, composite materials are susceptible to premature failure during their service time due to the stress concentration around voids or fibers leading to the formation of cracks or micro-cracks. The evolution of these cracks often leads to catastrophic failures [1, 2, 3]. Therefore, the determination of the stress fields near a hole or an inclusion (in an elastic plane) is a key problem for the engineering design of high-strength composite materials [4].

The problem of stress concentration around holes or inclusions under plane and anti-plane loading has been under intense investigation [5, 6, 7, 8, 9, 10] but mostly analytical solutions have been derived primarily for an infinite plane subject to uniform loading conditions. An experimental proof of stress concentrations around circular holes has been provided in [5, 11] and around polygonal inclusions in [12, 13] through photoelastic experiments. In addition, real world experiments on mortar specimens containing cylindrical inclusions have been conducted in [14] showing that the stress concentrations lead to crack openings around the inclusion.

Let us now restrict our attention to the problem of anti-plane elasticity which sometimes is considered to be a sort of a mathematical abstraction, yet the anti-plane problem of an inclusion embedded in an infinite elastic plane is fundamental in fiber-reinforced composites and crack problems [15]. Some simple real life examples of anti-plane problems are reported in detail in [16]. Most often, the anti-plane problem of an inclusion has been investigated with respect to uniform boundary conditions [17, 18, 19, 20, 21, 22, 23]. Nevertheless, nonuniform loadings have also been taken into account by [24, 25, 26, 27, 28, 29, 30, 31, 32]. Recently, the problem of a circular void and a rigid inclusion embedded in a bounded domain (annulus) subject to uniform and nonuniform anti-plane shear has been solved analytically in [16]. Moreover, multiple inclusions embedded in an infinite plane subject to uniform anti-plane shear have been analyzed in [33, 34, 35].

Though the problem of an elliptical hole in an infinite plane subject to uniform anti-plane shear load has been thoroughly investigated in [36], herein we extend the solution for nonuniform loading conditions (an infinite class of m th-order polynomials). Our solution covers both void and rigid inclusions, together with a crack or a rigid line inclusion (stiffener) obtained in the limit (when the minor axis of an ellipse tends to zero).

Despite the fact that nowadays different kinds of linear and nonlinear mechanical and physical problems can be solved numerically by an increasing number of powerful computer methods, closed-form solutions are still widely preferred over the numerical solutions mainly for two reasons. Firstly, analytical solutions can be used as benchmarks for validating the numerical results. Secondly, and more importantly, analytical solutions often lead to meaningful physical insights into the problem under consideration which may sometimes reveal some surprising and counter-intuitive features of the general solution.

Keeping in mind the above-mentioned facts, we first derive an analytical solution in terms of a complex potential through the method of analytic function together with a conformal mapping, and then we obtain the closed-form expression of Stress Concentration Factor (SCF) for both void and rigid elliptical inclusions forming the core of an infinite plane. While for a finite plane, a numerical solution is obtained by exploiting the heat-stress analogy via the finite element method. A comparison between the analytical

and numerical values of the SCFs for an elliptical inclusion and Stress Intensity Factors (SIFs) for a line inclusion show that the analytical solution of an infinite plane can be used as an accurate approximation to the case of a finite plane. Finally, the numerical analysis is extended to the problem of a crack or a stiffener by calculating the corresponding SIF values via the heat–stress analogy and finite element method by exploiting the concept of J-integral. In particular, the proposed methodology can easily handle the study of complex loading conditions and even interactions among inclusions and/or cracks. At last, a three-dimensional validation completes the analysis.

The paper is organized as follows: In Section 2, we present the problem governing equations and polynomial loading conditions in an anti-plane elasticity setting. In Section 3, we derive an analytical solution in terms of a closed-form complex potential and SCFs for an elliptical inclusion embedded in an infinite plane subject to uniform and nonuniform anti-plane shear loads. In Section 4, we focus on the numerical solution through the finite element method for the two-dimensional model by exploiting the heat–stress analogy and then extend the numerical analysis to a three-dimensional validation model. Finally, we compare the numerical results with the analytical findings and show that the analytical solution for an infinite plane can be safely used for a finite plane when the size of the inclusion is less than or equal to five.

2 Anti-plane problem governing equations and polynomial loading condition

Let us consider the case of anti-plane deformation in a Cartesian coordinate system (x, y, z) with the displacement field taking the form

$$u_x = u_y = 0, \quad u_z = w(x, y). \quad (1)$$

Consequently, the only non-zero shear stress components are given by constitutive equations through shear modulus μ and the gradient of the displacement field w as

$$\tau_{xz} = \mu w_{,x}, \quad \tau_{yz} = \mu w_{,y}, \quad (2)$$

where the differentiation with respect to variables x and y is denoted by comma. The stress field (2) in the absence of body forces must satisfy the equilibrium and compatibility equations

$$\tau_{xz,x} + \tau_{yz,y} = 0, \quad \tau_{xz,y} - \tau_{yz,x} = 0, \quad (3)$$

or in other words, the well-known Laplace equation and the Schwarz theorem for non-zero displacement field w , as

$$\nabla^2 w = w_{,xx} + w_{,yy} = 0, \quad w_{,xy} = w_{,yx}. \quad (4)$$

At last, the modulus of the shear stress can be obtained as a positive eigenvalue of the stress tensor in the form

$$\tau = \sqrt{(\tau_{xz})^2 + (\tau_{yz})^2}. \quad (5)$$

Following [29, 30], an infinite class of nonuniform force boundary conditions for out-of-plane problems is considered through the following polynomial series of m -th order ($m \in \mathbb{N}$) for remote shear stress components ($\bar{\tau}_{iz}$ with $i = x, y$)

$$\bar{\tau}_{xz}^{(m)}(x, y) = \sum_{j=0}^m b_j^{(m)} x^{m-j} y^j, \quad \bar{\tau}_{yz}^{(m)}(x, y) = \sum_{j=0}^m c_j^{(m)} x^{m-j} y^j, \quad (6)$$

where constants $b_j^{(m)}$ and $c_j^{(m)}$ ($j = 1, \dots, m$) are related to the two loading coefficients $b_0^{(m)}$ and $c_0^{(m)}$ through

$$\begin{aligned} b_j^{(m)} &= \frac{(-1)^{\lfloor j/2 \rfloor} m!}{2j! (m-j)!} \left[b_0^{(m)} [1 + (-1)^j] + c_0^{(m)} [1 - (-1)^j] \right], \\ c_j^{(m)} &= \frac{(-1)^{\lceil j/2 \rceil} m!}{2j! (m-j)!} \left[b_0^{(m)} [1 - (-1)^j] + c_0^{(m)} [1 + (-1)^j] \right], \end{aligned} \quad (7)$$

where symbols $\lfloor \cdot \rfloor$ and $\lceil \cdot \rceil$ stand, respectively, for floor and ceiling functions, while symbol $!$ represents the factorial function. Moreover, $b_0^{(m)}$ and $c_0^{(m)}$ are two constants defining the boundary condition for each order m of the polynomial and represent a measure of the remote shear stress. For instance, the shear stress state along the x_1 -axis takes the following form:

$$\bar{\tau}_{xz}^{(m)}(x, 0) = b_0^{(m)} x^m, \quad \bar{\tau}_{yz}^{(m)}(x, 0) = c_0^{(m)} x^m. \quad (8)$$

In case $m = 0$, loading constants $b_0^{(0)}$ and $c_0^{(0)}$ are usually called uniform anti-plane shear or Mode III loading, see Figure 1 in [29]. Finally, one can obtain the modulus of the shear stress (5) in polar coordinates, obtained from equation (14) in [29], which results to be independent of the circumferential angle θ ,

$$\bar{\tau}^{(m)}(r) = r^m \sqrt{\left[b_0^{(m)} \right]^2 + \left[c_0^{(m)} \right]^2}. \quad (9)$$

Equation (9) will be useful in the calculation of SCF along the boundary of an ellipse. It is clear from equation (9) that the contour levels of the remote shear stress modulus are concentric circles centered at the origin of the axes.

In the following, we analyze the extreme cases of an elliptical inclusion covering both void (plus sign) and rigid (minus sign) inclusions distinguished by $\chi = \pm 1$. In what follows, the solution is obtained for the elliptical inclusion and its limiting cases. The symbol embedded within angle brackets is used as an apex to distinguish the problems and related physical quantities: elliptical inclusion $\langle 0 \rangle$ with the limit case of circular inclusion $\langle \circ \rangle$ and the limit case of line inclusion $\langle - \rangle$, the case of crack $\langle c \rangle$ and the case of stiffener $\langle s \rangle$. It is worth noting that in the following sections (3 and 4) we first analytically solve the problem of an elliptical void or a rigid inclusion embedded in an infinite plane subject to uniform and nonuniform anti-plane shear and then extend the solution by exploiting finite element analysis and the heat–stress analogy to a finite plane. Finally, by comparing the SCFs from both methods we show that the analytical solution for an infinite plane can be used in the case of a finite plane with great accuracy.

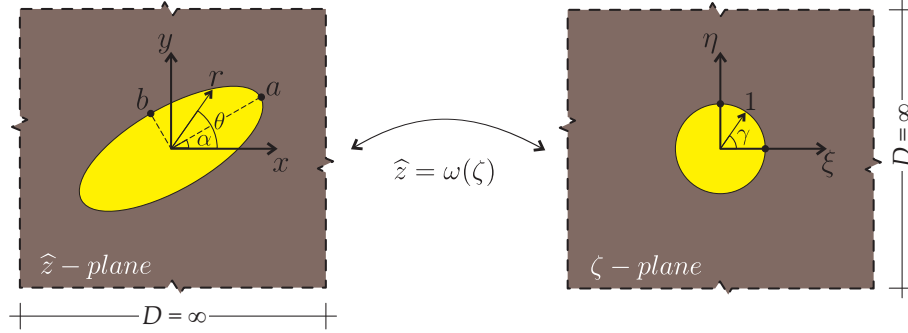


Figure 1: An elliptical inclusion embedded in an infinite plane, $D = \infty$, (namely the \hat{z} -plane) is mapped conformally via function $w(\zeta)$ onto a circular inclusion of unit radius embedded in an infinite plane (namely the ζ -plane).

3 Analytical solution for an elliptical inclusion embedded in an infinite plane

The full-field solution for the Laplace equation governing the anti-plane elastic problem is obtained through the complex potential technique together with a conformal mapping [6, 31]. An infinite plane containing an inclusion of a generic shape (\hat{z} -plane) is mapped onto an infinite plane containing a circular inclusion of a unit radius (ζ -plane), see Figure 1. The problem is formulated by introducing a complex potential $f^{(m)}(\hat{z})$, function of the complex variable $\hat{z} = x + iy$, with i denoting the imaginary unit. Due to the superposition principle, the complex potential $f^{(m)}(\hat{z})$ can be considered as a sum of an unperturbed complex potential $f_{\infty}^{(m)}(\hat{z})$ (when the inclusion is absent), and a perturbed potential $f_p^{(m)}(\hat{z})$ (perturbation induced by the inclusion). Finally, the complex potential $f^{(m)}(\hat{z})$ from the \hat{z} -plane can be transformed to the ζ -plane by using a mapping function $\hat{z} = \omega(\zeta)$ as

$$g^{(m)}(\zeta) = f^{(m)}(\omega(\zeta)). \quad (10)$$

For the sake of conciseness, some fundamental definitions are summarized in Table 1 for both planes.

The unperturbed complex potential $f_{\infty}^{(m)}(\hat{z})$ for each order m can be obtained by using the self-balanced remote polynomial stress field equation (6) as follows

$$f_{\infty}^{(m)}(\hat{z}) = T^{(m)}\hat{z}^{m+1}, \quad T^{(m)} = \frac{1}{m+1} \left(b_0^{(m)} - i c_0^{(m)} \right), \quad (11)$$

which for the particular case of a uniform anti-plane shear loading $m = 0$ returns equation (20) in [20].

Table 1: The correspondence among the physical quantities in both real (\widehat{z} -plane) and auxiliary plane (ζ -plane).

physical quantities	\widehat{z} -plane	ζ -plane
complex potential	$f^{(m)}(\widehat{z}) = f_{\infty}^{(m)}(\widehat{z}) + f_p^{(m)}(\widehat{z})$	$g^{(m)}(\zeta) = g_{\infty}^{(m)}(\zeta) + g_p^{(m)}(\zeta)$
displacement field	$w^{(m)}(\widehat{z}) = \frac{1}{\mu} \text{Re}[f^{(m)}(\widehat{z})]$	$w^{(m)}(\zeta) = \frac{1}{\mu} \text{Re}[g^{(m)}(\zeta)]$
stress field	$\tau_{xz}^{(m)}(\widehat{z}) - i\tau_{yz}^{(m)}(\widehat{z}) = f^{(m)'}(\widehat{z})$	$\tau_{xz}^{(m)}(\zeta) - i\tau_{yz}^{(m)}(\zeta) = \frac{g^{(m)'}(\zeta)}{\omega'(\zeta)}$
shear force resultant along an arc \widehat{BC}	$F_{\widehat{BC}}^{(m)}(\widehat{z}) = \text{Im} [f^{(m)}(\widehat{z}_C) - f^{(m)}(\widehat{z}_B)]$	$F_{\widehat{BC}}^{(m)}(\zeta) = \text{Im} [g^{(m)}(\zeta_B) - g^{(m)}(\zeta_C)]$

3.1 Conformal mapping and closed-form complex potential

Exterior region of an elliptical inclusion is transformed onto the exterior region of the unit circle by the mapping function [6]

$$\widehat{z}^{\langle 0 \rangle} = \omega^{\langle 0 \rangle}(\zeta) = e^{i\alpha} \left(\frac{1+k}{2} a \right) \left[\zeta + \left(\frac{1-k}{1+k} \right) \frac{1}{\zeta} \right], \quad (12)$$

with

$$k = \frac{b}{a} \in [0, 1], \quad (13)$$

denoting the aspect ratio of an ellipse with semi-major axis a and semi-minor axis b along x and y , respectively. Moreover, α denotes the angle of rotation of an ellipse in the \widehat{z} -plane, see Figure 1. The lower and upper bounds of parameter k represent a crack of length $2a$ and a circle of radius a respectively.

By using definition (11) and the binomial theorem, it is possible to write the unperturbed complex potential as

$$g_{\infty}^{(m)\langle 0 \rangle}(\zeta) = T^{(m)} \left(\frac{1+k}{2} a \right)^{m+1} e^{i\alpha(m+1)} \sum_{j=0}^{m+1} \frac{(m+1)!}{j!(m+1-j)!} \left(\frac{1-k}{1+k} \right)^j \zeta^{m+1-2j}. \quad (14)$$

Equation (14) is divided into a positive and a negative power series as

$$g_{\infty}^{(m)\langle 0 \rangle}(\zeta) = T^{(m)} \left(\frac{1+k}{2} a \right)^{m+1} e^{i\alpha(m+1)} \left[\sum_{j=0}^Q \frac{(m+1)!}{j!(m+1-j)!} \left(\frac{1-k}{1+k} \right)^j \zeta^{m+1-2j} + \sum_{j=Q+1}^{m+1} \frac{(m+1)!}{j!(m+1-j)!} \left(\frac{1-k}{1+k} \right)^j \frac{1}{\zeta^{2j-m-1}} \right], \quad (15)$$

where $Q \in \mathbb{N}_0$ is given by a floor function as

$$Q = \left\lfloor \frac{m+1}{2} \right\rfloor = 0, 1, 1, 2, 2, 3, 3, \dots, \quad \text{for } m = 0, 1, 2, 3, 4, 5, 6, \dots \quad (16)$$

It is worth noting that the numerical behavior of Q is fundamental in the SCF values. Imposing the null traction or displacement boundary condition along the unit circle in the conformal plane (ζ -plane) leads to a closed-form perturbed complex potential

$$g_p^{(m)\langle 0 \rangle}(\zeta) = \left(\frac{1+k}{2} a \right)^{m+1} \left[\chi \overline{T^{(m)}} e^{-i\alpha(m+1)} \left(\sum_{j=0}^Q \frac{(m+1)!}{j!(m+1-j)!} \left(\frac{1-k}{1+k} \right)^j \frac{1}{\zeta^{m+1-2j}} - \frac{(2Q)!}{Q!Q!} \left(\frac{1-k}{1+k} \right)^Q \delta_{2Q,m+1} \right) - T^{(m)} e^{i\alpha(m+1)} \sum_{j=Q+1}^{m+1} \frac{(m+1)!}{j!(m+1-j)!} \left(\frac{1-k}{1+k} \right)^j \frac{1}{\zeta^{2j-m-1}} \right]. \quad (17)$$

By using the superposition principle, the sum of the unperturbed (15) and perturbed (17) complex potentials leads to the closed-form expression of the complex potential as

$$g^{(m)\langle 0 \rangle}(\zeta) = \left(\frac{1+k}{2} a \right)^{m+1} \left[\sum_{j=0}^Q \frac{(m+1)!}{j!(m+1-j)!} \left(\frac{1-k}{1+k} \right)^j \left(T^{(m)} e^{i\alpha(m+1)} \zeta^{m+1-2j} + \chi e^{-i\alpha(m+1)} \frac{\overline{T^{(m)}}}{\zeta^{m+1-2j}} \right) - \chi \overline{T^{(m)}} e^{-i\alpha(m+1)} \frac{(2Q)!}{Q!Q!} \left(\frac{1-k}{1+k} \right)^Q \delta_{2Q,m+1} \right]. \quad (18)$$

For instance, for a non-rotated ($\alpha = 0$) elliptical void ($\chi = 1$) with aspect ratio ($k = 1/3$) the complex potential (18) takes the following forms for uniform, linear and quadratic ($m = 0, 1, 2$) anti-plane shear loads, respectively;

$$\begin{aligned} g^{(0)\langle 0 \rangle}(\zeta) &= \frac{2}{3} a \left(T^{(0)} \zeta + \frac{\overline{T^{(0)}}}{\zeta} \right), \\ g^{(1)\langle 0 \rangle}(\zeta) &= \frac{4}{9} a^2 \left(T^{(1)} (\zeta^2 + 1) + \frac{\overline{T^{(1)}}}{\zeta^2} \right), \\ g^{(2)\langle 0 \rangle}(\zeta) &= \frac{4}{9} a^3 \left(T^{(2)} \zeta + \frac{\overline{T^{(2)}}}{\zeta} \right) + \frac{8}{27} a^3 \left(T^{(2)} \zeta^3 + \frac{\overline{T^{(2)}}}{\zeta^3} \right). \end{aligned} \quad (19)$$

Equation (18) simplifies according to the two physical limits of an ellipse, namely, a circle and a line inclusion, as follows: $k = 1$ corresponds to a circular inclusion of radius a and gives

$$g^{(m)\langle 0 \rangle}(\zeta) = a^{m+1} \left[T^{(m)} e^{i\alpha(m+1)} \zeta^{m+1} + \chi e^{-i\alpha(m+1)} \frac{\overline{T^{(m)}}}{\zeta^{m+1}} \right]. \quad (20)$$

It is worth mentioning that the solution does not depend on angle α due to an infinite number of axes of symmetry of the circle. Therefore, equation (21) simplifies to

$$g^{(m)(\circ)}(\zeta) = a^{m+1} \left[T^{(m)} \zeta^{m+1} + \chi \frac{\overline{T^{(m)}}}{\zeta^{m+1}} \right], \quad (21)$$

which for uniform anti-plane shear case ($m = 0$) turns into the case investigated in [20, 29, 22]. For $k = 0$, corresponding to a line inclusion, i.e., a crack or a stiffener of length $2a$, the complex potential takes the following form:

$$g^{(m)(-)}(\zeta) = \left(\frac{a}{2}\right)^{m+1} \left[\sum_{j=0}^Q \frac{(m+1)!}{j!(m+1-j)!} \left(T^{(m)} e^{i\alpha(m+1)} \zeta^{m+1-2j} + \chi e^{-i\alpha(m+1)} \frac{\overline{T^{(m)}}}{\zeta^{m+1-2j}} \right) - \chi e^{-i\alpha(m+1)} \overline{T^{(m)}} \frac{(2Q)!}{Q!Q!} \delta_{2Q,m+1} \right], \quad (22)$$

which for uniform anti-plane shear ($m = 0$) and null rotation ($\alpha = 0$) turns to the case studied in [20, 29].

An example of the full-field solution (18) for an elliptical inclusion having aspect ratio $k = 1/3$ and being subject to uniform anti-plane shear ($b_0^{(0)} = 0$ for a void or $c_0^{(0)} = 0$ for a rigid inclusion) is reported in Figure 2. The contour plots of the modulus of the shear stress show that the position of maximum shear stress does not remain at the tip of the ellipse but moves according to the angle of rotation (α) of the inclusion. Moreover, the stress concentration decreases along with an increase in angle α , as expected. In particular, stress concentration values $\text{SCF} \cong \{4, 3.83, 3.33, 2.59, 1.77, 1.33\}$ are obtained for angles with constant interval $\alpha = \{0^\circ, 18^\circ, 36^\circ, 54^\circ, 72^\circ, 90^\circ\}$, respectively. The angle of the maximum SCF in the first quadrant is given by $\theta \cong \{0^\circ, 17.3^\circ, 34.4^\circ, 51.1^\circ, 65.5^\circ, 0^\circ\}$, respectively.

3.2 Stress concentration factors

Closed-form expression for the stress concentration factors for an elliptical void, or an elliptical rigid inclusion, embedded in an infinite plane is derived in this section for each m through the well-known definition:

$$\text{SCF}_\infty^{(m)}(\theta, \alpha) = \frac{\tau^{(m)}(\theta, \alpha)}{\overline{\tau}^{(m)}(\theta, \alpha)}, \quad (23)$$

where angles α and θ are defined in Figure 1. Moreover, subscript ∞ of SCF denotes the analytical solution for an infinite plane. By using the equations provided in Table 1, equation (5) and by knowing that

$$\sum_{j=0}^Q \frac{(m+1-2j)}{j!(m+1-j)!} \left(\frac{1-k}{1+k}\right)^j \geq 0, \quad \forall m, \quad (24)$$

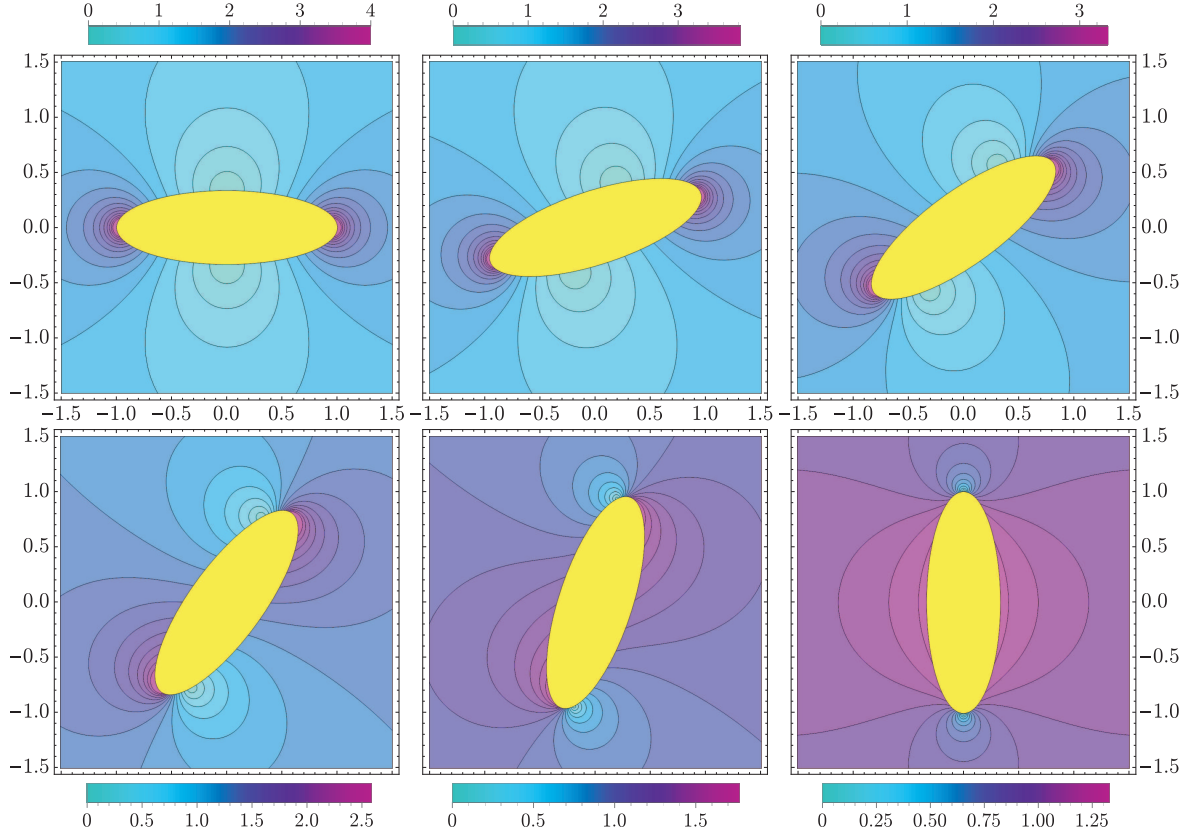


Figure 2: Full-field solution in terms of the modulus of shear stress as a contour plot for an elliptical inclusion ($k = 1/3$), with different rotation angles α , embedded in an infinite plane subject to uniform ($m = 0$) anti-plane shear ($b_0^{(0)} = 0$ for a void or $c_0^{(0)} = 0$ for a rigid inclusion).

it is possible to obtain the modulus of shear stress $\tau^{(m)\langle 0 \rangle}(\gamma, \alpha)$ in the conformal plane as

$$\tau^{(m)\langle 0 \rangle}(\gamma, \alpha) = \frac{(m+1)! a^m (1+k)^{m+1} \left| \mathcal{F}_j^{(m)}(\gamma, \alpha) \right|}{(m+1) 2^{m+\frac{1}{2}} \sqrt{k^2+1} + (k^2-1) \cos(2\gamma)} \sum_{j=0}^Q \frac{(m+1-2j)}{j! (m+1-j)!} \left(\frac{1-k}{1+k} \right)^j, \quad (25)$$

where symbol $|\cdot|$ represents the absolute value of the given function. Angle γ is defined in Figure 1, while angular function $\mathcal{F}_j^{(m)}(\gamma, \alpha)$ is given by the following expression:

$$\mathcal{F}_j^{(m)}(\gamma, \alpha) = \left[\begin{aligned} & \left[(b_0^{(m)}(1-\chi) + c_0^{(m)}(\chi+1)) \cos((m+1-2j)(\gamma+\alpha)) \right. \\ & \left. - \left[(\chi-1)c_0^{(m)} + b_0^{(m)}(\chi+1) \right] \sin((m+1-2j)(\gamma+\alpha)) \right] \end{aligned} \right] \quad (26)$$

The modulus of the shear stress in (25) can be transformed onto the elliptical contour in the physical plane by exploiting the relationship between angle γ in the ζ -plane and

angle θ in the \widehat{z} -plane:

$$\tan \gamma = \frac{1}{k} \tan(\theta - \alpha), \quad (27)$$

therefore angle γ is written as $\gamma = \arctan[k \cos(\theta - \alpha), \sin(\theta - \alpha)]$, where the trigonometric function $\arctan[x, y]$ gives arcus tangent of y/x . It should be noted that for the particular case of a circular inclusion ($k = 1$) the modulus of shear stress in the physical plane simplifies to

$$\begin{aligned} \tau^{(m)\langle 0 \rangle}(\theta) = a^m & \left| \left[b_0^{(m)}(1 - \chi) + c_0^{(m)}(\chi + 1) \right] \cos((m + 1)\theta) \right. \\ & \left. - \left[(\chi - 1)c_0^{(m)} + b_0^{(m)}(\chi + 1) \right] \sin((m + 1)\theta) \right|. \end{aligned} \quad (28)$$

By using the definition of the modulus of the principle shear stress in (9), it is possible to obtain the unperturbed shear stress along the congruent ellipses contour in the \widehat{z} -plane as

$$\bar{\tau}^{(m)\langle 0 \rangle}(\theta, \alpha) = \left(\frac{k a}{\sqrt{k^2 \cos^2(\theta - \alpha) + \sin^2(\theta - \alpha)}} \right)^m \sqrt{\left(b_0^{(m)} \right)^2 + \left(c_0^{(m)} \right)^2}. \quad (29)$$

Finally, by putting together equations (23), (25), (27) and (29) one can obtain the final formula for the stress concentration in the physical plane. Due to the limited space, we do not report the final general expression of the SCF but only one of the most significant cases. For instance, when the inclusion rotation is disregarded ($\alpha = 0$) the SCF at the tip ($\theta = 0$) of the ellipse takes the form

$$\text{SCF}_\infty^{(m)\langle 0 \rangle}(0, 0) = \frac{(m + 1)! (k + 1)^{m+1} \left| (1 + \chi)c_0^{(m)} + (1 - \chi)b_0^{(m)} \right|}{(m + 1)k 2^{m+1} \sqrt{\left(b_0^{(m)} \right)^2 + \left(c_0^{(m)} \right)^2}} \sum_{j=0}^Q \frac{(m + 1 - 2j)}{j! (m + 1 - j)!} \left(\frac{1 - k}{1 + k} \right)^j. \quad (30)$$

It should be noted that for the case of a hole ($\chi = 1$) with the corresponding loading condition ($b_0^{(m)} = 0$) or for the case of a rigid inclusion ($\chi = -1$) with the corresponding loading condition ($c_0^{(m)} = 0$) equation (30) simplifies to

$$\text{SCF}_\infty^{(m)\langle 0 \rangle}(0, 0) = \frac{(m + 1)! (k + 1)^{m+1}}{(m + 1)k 2^m} \sum_{j=0}^Q \frac{(m + 1 - 2j)}{j! (m + 1 - j)!} \left(\frac{1 - k}{1 + k} \right)^j, \quad (31)$$

which for the case of uniform anti-plane shear loading ($m = 0$) returns equation (50) derived in [22]. In addition, it is worth mentioning that at the limit $m \rightarrow \infty$ for a fixed $k \neq 0$, equation (31) returns $\text{SCF} = 2$.

Analytical formulae obtained from equation (30) are reported in Table 2 for different loading orders $m = 0, 1, 2, \dots, 10$. It should be noted that the SCF values for void and rigid inclusions are the same but the loadings are switched. This feature is due to the analogy between void and rigid inclusions explained in detail in [29]. While the overall behavior of the SCFs is depicted in Figure 3 showing that when $k \rightarrow 1$ (a circular hole)

the SCF value tends to value 2 as in [16, 20, 29, 22]. On the other hand, when $k \rightarrow 0$ (a crack) then the value of SCF explodes to infinity, so that the definition of stress intensity factor is needed. It is worth mentioning that in Table 2 and Figure 3 one can notice that unlike the uniform case each pair of order m produces the same SCF value. This peculiar behavior stems from the floor function of parameter Q in equation (16).

Table 2: Analytical formulae for the SCFs covering both void and rigid inclusions (for void ($\chi = 1$) with $b_0^{(m)} = 0$, for rigid ($\chi = -1$) with $c_0^{(m)} = 0$). In particular, the inclusion rotation is ignored, i.e., $\alpha = 0$, and the body is subject to a uniform or nonuniform anti-plane loading with $m = 0, 1, 2, \dots, 10$).

m	$\text{SCF}_\infty^{(m)\langle 0 \rangle}(0, 0)$
0 [22]	$\frac{k+1}{k}$
1&2	$\frac{k+1}{k} \left[\frac{k+1}{2} \right]$
3&4	$\frac{k+1}{k} \left[\frac{(k+1)^2(3-k)}{8} \right]$
5&6	$\frac{k+1}{k} \left[\frac{(k+1)^3(k^2-4k+5)}{16} \right]$
7&8	$\frac{k+1}{k} \left[\frac{(k+1)^4(5k^3-25k^2+47k-35)}{128} \right]$
9&10	$\frac{k+1}{k} \left[\frac{(k+1)^5(7k^4-42k^3+102k^2-122k+63)}{256} \right]$

3.3 Stress intensity factors

According to [30, 32], the stress intensity factors for the symmetric and antisymmetric anti-plane problems are defined, respectively, as

$$K_{\text{III}}^{(s)} = \lim_{\rho \rightarrow 0} \sqrt{2\pi\rho} \tau_{\rho 3}(\rho, 0), \quad K_{\text{III}}^{(c)} = \lim_{\rho \rightarrow 0} \sqrt{2\pi\rho} \tau_{\theta 3}(\rho, 0), \quad (32)$$

where $\langle s \rangle$ and $\langle c \rangle$ refer to a stiffener and crack, respectively. While ρ represents the radial distance from the crack tip. Let us consider a line inclusion ($k = 0$) of length $2a$ with null rotation ($\alpha = 0$). The asymptotic stress field and the inverse mapping procedure given in [30] yield the following analytical formula for the stress intensity factors for each loading order m :

$$\begin{bmatrix} K_{\text{III}\infty}^{(m)\langle s \rangle} \\ K_{\text{III}\infty}^{(m)\langle c \rangle} \end{bmatrix} = \frac{\sqrt{\pi a}}{2^m(m+1)} \sum_{j=0}^Q \frac{(m+1)!(m+1-2j)}{j!(m+1-j)!} \begin{bmatrix} \bar{\tau}_{xz}^{(m)}(a, 0) \\ \bar{\tau}_{yz}^{(m)}(a, 0) \end{bmatrix}. \quad (33)$$

It is worth mentioning that when a stiffener is subject to antisymmetric and a crack is subject to symmetric loading no singularity is activated in both cases meaning that both

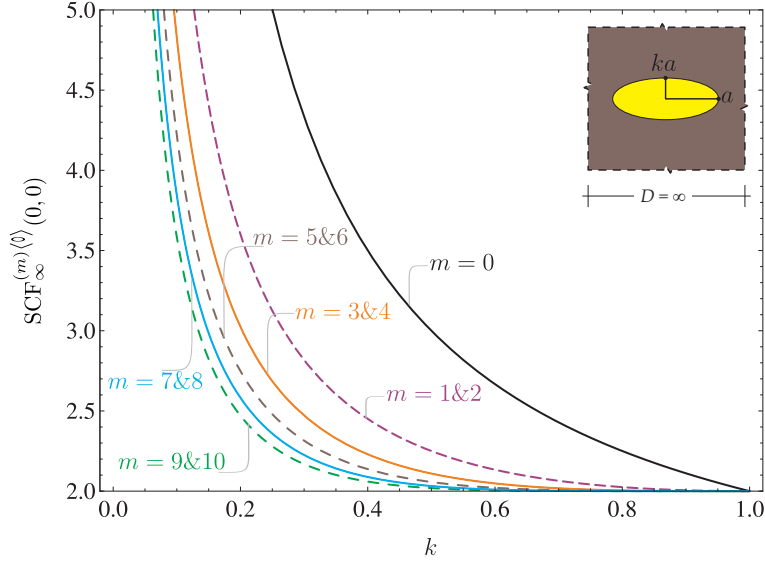


Figure 3: Overall graphical behavior of the analytical SCF values (Table 2) for the extreme cases of an elliptical inclusion. In particular, the inclusion rotation is ignored, i.e., $\alpha = 0$, and the body is subject to a uniform or nonuniform anti-plane loading with $m = 0, 1, 2, \dots, 10$.

SIFs are identically zero. For a more detailed explanation, please see Section 2.2 of [29]. Moreover, it should be noted that subscript ∞ of K_{III} denotes the analytical solution for an infinite plane.

4 Comparison between analytical and numerical results and three-dimensional model validation

4.1 Two-dimensional model and heat–stress analogy

The governing equations in anti-plane elasticity and two-dimensional thermal conduction [40] are mathematically identical, see Table 2 in [16]. Therefore, stress analysis is conducted by solving a 2D heat conduction problem within the finite element method (FEM) software Comsol Multiphysics[®] (version 4.2a). The results for an infinite plane are confirmed by taking a plane 10 times bigger than the inclusion. The stress analysis is finally extended to the crack or stiffener problem through the concept of J-integral.

To solve the problem, we select the heat transfer module within the software with stationary study and two-dimensional space. We choose the built-in basic elastic material with Young’s modulus E and shear modulus G (equivalent to μ) as the material properties of the physical space. For the case of a void, a null traction vector boundary condition along the ellipse contour is imposed, which is fulfilled by selecting the open boundary option available in the model. Whereas for the rigid inclusion problem, a zero temperature (null displacement) boundary condition along the ellipse contour is imposed.

The whole domain is meshed by using the user-controlled mesh option with custom-free triangular element size at two levels. At the first level, the domain is meshed with the

maximum element size of $0.05 D$ (with D being the side length of the square enclosure). At the second level, the boundaries of the elliptical hole are meshed with the maximum element size of $0.01 D$. At last, convergence is checked for the accuracy of the geometry and the solution field.

The comparison between the analytical solution obtained for an elliptical or a line inclusion embedded in an infinite plane and the numerical results for the corresponding finite plane using FEM is made through the concept of percent error $\%_{error}$ defined as

$$\%_{error} = \left| \frac{V_{numerical} - V_{analytic}}{V_{numerical}} \right| \times 100, \quad (34)$$

where V stands for any analytical or numerical scalar value.

In Table 3, we present the numerical SCF values for an elliptical inclusion embedded in a square-shaped finite domain and a comparison between the numerical and analytical values is reported according to (34). When the error is less than 3 percent, it is highlighted in bold. The study is carried out for various aspect ratios $D/(2a)$ and k with uniform and nonuniform anti-plane plane conditions ($b_0^{(0)} = 0$ for a void and $c_0^{(0)} = 0$ for a rigid inclusion) and for different loading orders $m = 0, 1, 2$.

4.2 SCFs: infinite plane vs finite plane

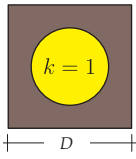
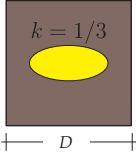
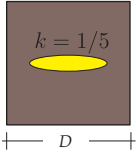
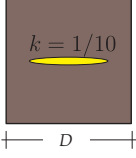
For an elliptical inclusion (with different aspect ratios $k = 1, 1/3, 1/5, 1/10$) embedded in a square-shaped finite domain (with varying dimensions $D/(2a) = 1.5, 2, 3, 4, 5$) subject to uniform and nonuniform anti-plane plane loading ($b_0^{(0)} = 0$ for a void and $c_0^{(0)} = 0$ for a rigid inclusion) under different loading orders $m = 0, 1, 2, 3, 4$, the overall behavior of the dimensionless SCF values is depicted in Figure 4. In Table 3, in turn, we present a comparison between the analytical SCF values for an infinite domain and the numerical values for a finite domain, through the concept of percent error given in equation (34). The results lead to the following observations:

- The case of uniform loading ($m = 0$) produces the most severe stress concentrations.
- Only for the circular inclusion, the SCF values decrease monotonically along with an increase in the loading order m .
- For an elliptical inclusion, instead of monotonically increasing, the SCF values oscillate according to the even and odd loading orders: $SCF_D^{(0)} > SCF_D^{(2)} > SCF_D^{(4)} > SCF_D^{(1)} > SCF_D^{(3)}$.
- Surprisingly, for aspect ratio as small as $D/(2a) = 5$, the error is already approximately equal or less than 3 %, see Table 3 (entries highlighted in bold) and Figure 5. Therefore, the analytical solution of an infinite plane can be used as an accurate approximation to the case of a finite plane already for lower aspect ratios than $D/(2a) \geq 10$ generally considered as a realistic engineering limit for the infinite plane hypothesis.

- The analytical prediction for the existence of two stress annihilation points at $\theta = \pi/2, 3/2\pi$ is confirmed numerically for an elliptical void with aspect ratio $k = 1/3$ embedded in a finite square plane (with $D/(2a) = 5$) subject to uniform ($m = 0$) anti-plane shear ($c_0^{(0)}$), see Figure 5.

It is worth mentioning that the above-listed results can be considered to be relevant for the engineering design processes of the fast running world, as ready-made analytical formulae are preferred to time-consuming and computationally costly numerical analysis.

Table 3: Numerical SCF values (subscript D indicates the numerical solution for finite domains) for an elliptical inclusion embedded in a square-shaped finite plane, with varying aspect ratios $D/2a$ and k , subject to uniform and nonuniform anti-plane plane shear ($b_0^{(0)} = 0$ for a void or $c_0^{(0)} = 0$ for a rigid inclusion) with loading orders $m = 0, 1, 2$. (Bold highlights that the percent error is less than 3%.)

cross-section	$D/(2a)$	$\text{SCF}_D^{(0)\langle 0 \rangle}(0, 0)$	$\%_{error}$	$\text{SCF}_D^{(1)\langle 0 \rangle}(0, 0)$	$\%_{error}$	$\text{SCF}_D^{(2)\langle 0 \rangle}(0, 0)$	$\%_{error}$
	1.5	3.48362	42.6	2.45472	18.5	2.18321	8.3
	2	2.59180	22.9	2.11990	5.7	2.18199	1.6
	3	2.21817	9.8	2.02228	1.1	2.03269	0.2
	4	2.11552	5.5	2.00702	0.3	2.00106	0.1
	5	2.07198	3.5	2.00290	0.1	2.00047	0.0
	1.5	5.74030	30.3	2.81249	5.1	3.08833	13.7
	2	4.73766	15.6	2.70651	1.4	2.83744	6.0
	3	4.28149	6.6	2.67478	0.3	2.73107	2.3
	4	4.15141	3.6	2.66977	0.1	2.70167	1.3
	5	4.09512	2.3	2.66841	0.0	2.68906	0.8
	1.5	8.24163	27.2	3.74732	3.9	4.16855	13.6
	2	6.97222	13.9	3.64032	1.1	3.83994	6.2
	3	6.37496	5.9	3.60810	0.2	3.69234	2.5
	4	6.20160	3.3	3.60291	0.1	3.65025	1.4
	5	6.12624	2.1	3.60155	0.0	3.63208	0.9
	1.5	14.62243	24.8	6.24673	3.1	6.98105	13.3
	2	12.60267	12.7	6.10232	0.9	6.45220	6.2
	3	11.62290	5.4	6.05814	0.1	6.20432	2.5
	4	11.33498	2.9	6.05120	0.0	6.13255	1.3
	5	11.20904	1.9	6.04929	0.0	6.10126	0.8

4.3 SIFs: infinite plane vs finite plane

The concept of J -integral [39] has been thoroughly exploited in what follows for the crack problem in order to calculate the stress intensity factor for the specific given boundary value problem. J -integral for a plane problem is defined as

$$J = \oint_C \left(W dy - \mathbf{T} \cdot \frac{\partial \mathbf{u}}{\partial x} ds \right), \quad (35)$$

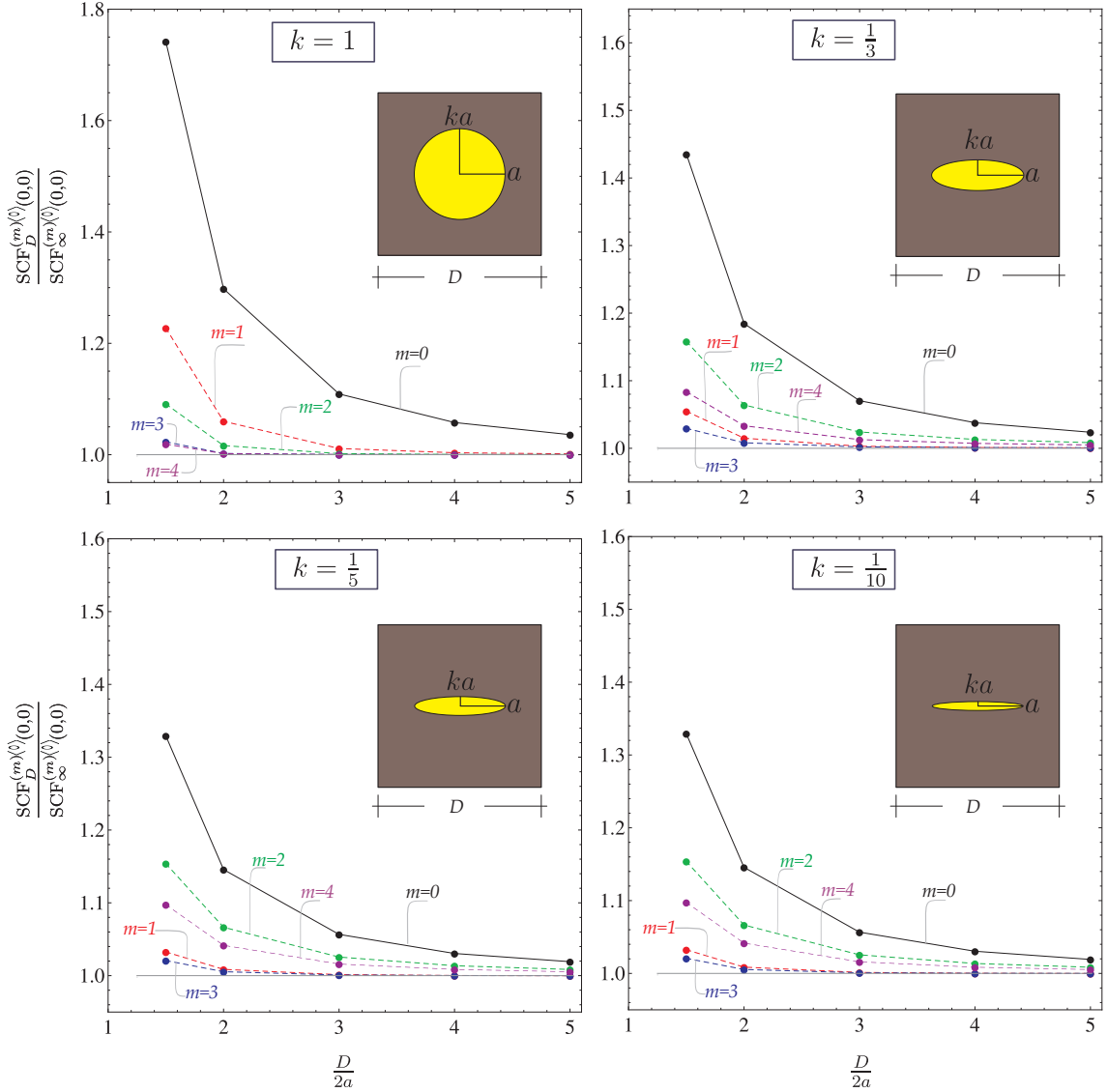


Figure 4: Dimensionless SCF values for both void and rigid elliptical inclusions. In particular, the inclusion with rotation is ignored, i.e., $\alpha = 0$ and the body is subject to uniform and nonuniform anti-plane shear with $m = 0, 1, 2, \dots, 10$. Unlike in the uniform case, each pair of m produces the same SCF value due to equations (16) and (30). The SCF value 2 is obtained for a circular void ($k = 1$) subject to any loading order, as shown in [30]. When $k \rightarrow 0$, a line inclusion is obtained and the value of SCF tends to infinity.

where \mathcal{C} denotes any counterclockwise contour surrounding the crack tip, s stands for the curvilinear coordinate along the contour \mathcal{C} , W denotes the strain-energy density, \mathbf{T} represents a traction vector defined according to the outward normal to the contour, and \mathbf{u} denotes the displacement vector. However, if we restrict our attention to the anti-plane problem under consideration the classical definition of mode-III J -integral for

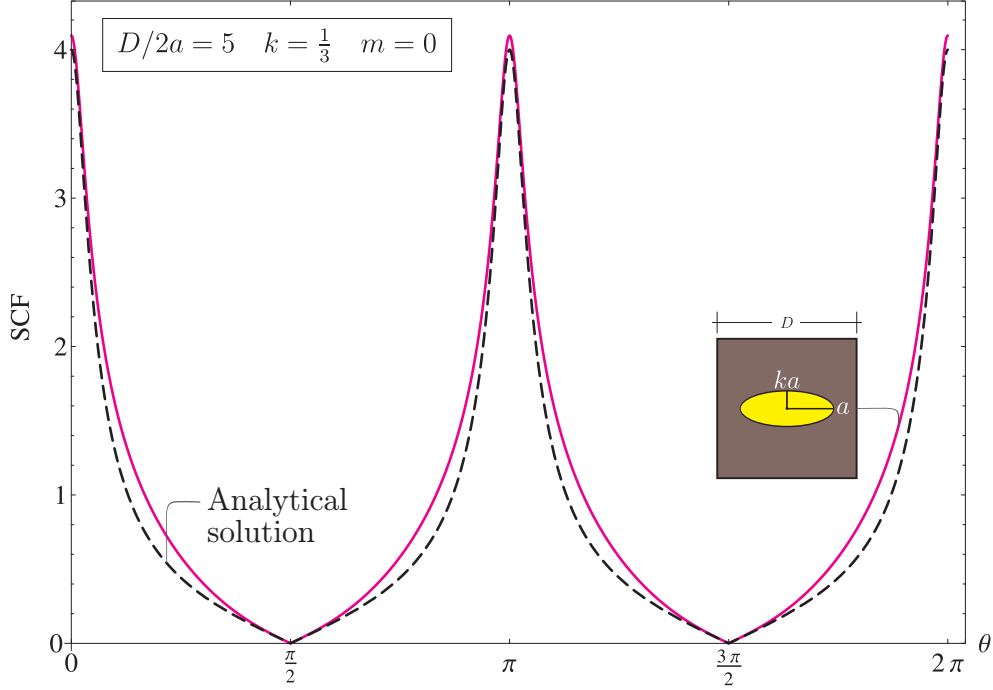


Figure 5: Analytical predictions of maximum SCF values 4 at the tip of an ellipse ($\theta = 0$) with the 2 peculiar stress annihilation points at $\theta = \pi/2, 3/2\pi$ are confirmed numerically for an elliptical void with aspect ratio $k = 1/3$ embedded in a finite square plane having length $D/(2a) = 5$ (similar result is also obtained for torsion problem in [37]) when subject to uniform ($m = 0$) anti-plane shear ($c_0^{(0)}$).

out-of-plane states leads to the following integral expression:

$$J_{\text{III}} = \oint_{\mathcal{C}} \left[\left(\frac{\tau_{xz}^2 + \tau_{yz}^2}{2\mu} \right) n_x - (\tau_{xz}n_x + \tau_{yz}n_y) \frac{\partial w(x, y)}{\partial x} \right] ds. \quad (36)$$

Here n_x and n_y denote the Cartesian components of the outward unit normal to contour \mathcal{C} along the x - and y -directions, respectively. It is worth mentioning that term $\partial w(x, y)/\partial x$ is equivalent to τ_{xz}/μ as per equation (2), therefore

$$J_{\text{III}} = \frac{1}{2\mu} \oint_{\mathcal{C}} [(\tau_{yz}^2 - \tau_{xz}^2) n_x - 2(\tau_{yz}\tau_{xz}) n_y] ds. \quad (37)$$

Considering the asymptotic behavior of the kinematic and stress fields, equation (36) reduces to the following relation connecting the J -integral to the well known SIF [38]:

$$K_{\text{III}} = \sqrt{2\mu J_{\text{III}}}. \quad (38)$$

Equation (38) represents a key tool in the evaluation of the SIF and is used in combination with finite element analysis in the next subsection in order to confirm the theoretical SIF values of (33) for an infinite plane, considered valid for a finite plane as well (under certain assumptions). For the sake of clarity and completeness, in Appendix we have

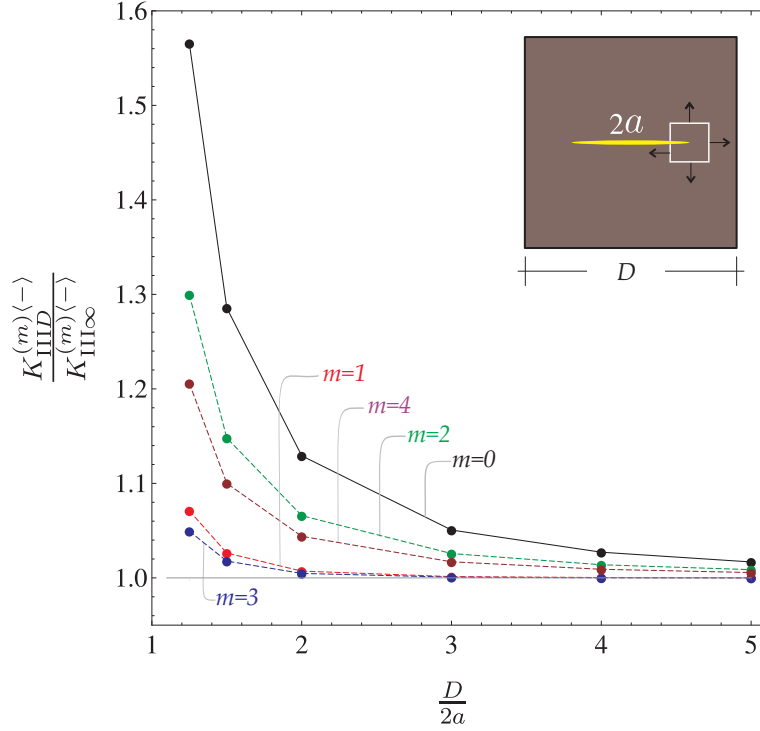


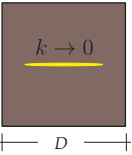
Figure 6: Dimensionless values of SIFs for both a crack and a stiffener are presented, in particular when the line inclusion (distinguished by the symbol $\langle - \rangle$) has null rotation ($\alpha = 0$). The system is subject to uniform and nonuniform ($m = 0, 1, 2, 3, 4$) anti-plane loading conditions ($b_0^{(0)} = 0$ for a void or $c_0^{(0)} = 0$ for a rigid inclusion).

given the derivation of the stress intensity factor for a crack of length $2a$ embedded in an infinite elastic plane subject to uniform loading.

For the numerical evaluation of the stress intensity factor for finite domains, we have considered a square contour surrounding a crack tip defined by the corresponding normals, see Figure 6, at the definition level of the model within the heat transfer module. Moreover, at the same level, integration operator (37) is defined. In the post-processing part, a global evaluation of the SIF from the derived values is recovered. The SIF values for a crack or a stiffener ($k = 0$) embedded in a square-shaped finite domain (with aspect ratios $D/(2a) = 1.25, 1.5, 2, 3, 4, 5$) subject to uniform and nonuniform anti-plane plane shear ($b_0^{(0)} = 0$ for a void or $c_0^{(0)} = 0$ for a rigid inclusion) with loading orders $m = 0, 1, 2, 3, 4$ is analyzed and, accordingly, the overall behavior of the dimensionless SIF values for the finite domain is graphically depicted in Figure 6. In Table 4, we present a comparison between the analytical SIF values for an infinite domain and the numerical values for a finite domain, through the concept of percent error given in equation (34). The results show the following:

- Similarly to the case of an elliptical inclusion, the SIF values for a line inclusion oscillate as a function of even and odd loading orders.
- Slightly differently to the case of an elliptical inclusion, already for aspect ratio

Table 4: Numerical SIF values for a line inclusion (distinguished by the symbol $\langle - \rangle$) embedded in a square-shaped finite plane, with varying aspect ratios $D/(2a)$ subject to uniform and nonuniform anti-plane plane condition ($b_0^{(0)} = 0$ for a void or $c_0^{(0)} = 0$ for a rigid inclusion) with different loading order $m = 0, 1, 2$ are presented. (Bold font highlights that the percent error is less than 3%.)

cross-section	$D/(2a)$	$K_{\text{III}D}^{(0)\langle - \rangle}$	% _{error}	$K_{\text{III}D}^{(1)\langle - \rangle}$	% _{error}	$K_{\text{III}D}^{(2)\langle - \rangle}$	% _{error}
	1.25	1.56562	36.1	0.53553	6.6	0.64986	23.1
	1.5	1.28568	22.2	0.51316	2.6	0.57404	12.9
	2	1.12923	11.4	0.50359	0.7	0.53294	6.2
	3	1.05064	4.8	0.50067	0.1	0.51287	5.0
	4	1.02718	2.6	0.50019	0.0	0.50695	2.7
	5	1.01685	1.7	0.50007	0.0	0.50435	0.9

$D/(2a) = 4$ the error is less than 3 % (highlighted in bold in Table 4). Therefore, the analytical solution for an infinite plane can be safely used as an approximation for finite domains with aspect ratios $D/(2a) \geq 4$.

4.4 Three-dimensional model validation

Finally, we perform a three-dimensional stress analysis in order to illustrate the problem setting and for validating the (two-dimensional) plane model. We investigate an elliptical void with aspect ratio $k = 1/3$ embedded in a square enclosure (with side length $D = 3a$) subject to uniform anti-plane shear, see Figure 7. Due to symmetry, only one quarter of the domain is analyzed. The length of the square prism with a collinear elliptical void is set to about $7D$ leading to a stress field close to the corresponding stress field of the plane model. The plane on which the stress field is analyzed is placed in the middle of the longitudinal axis of the square prism. The three-dimensional model is meshed as follows: at first, the cross section is meshed with free-shaped quadrilateral finite elements together with local mesh refinements near the elliptical contour, then the mesh is swept along the longitudinal axis of the square prism (resulting in a hexahedral mesh, altogether 19400 finite elements). Moreover, we have checked the convergence of the finite element approximation through the comparison of the resulting SCF value aiming at a discretization error less than 0.01 %. A unit surface load is applied at the top horizontal edge of the model and it is defined as force per unit area, while the bottom horizontal edge is fixed. In addition, a symmetry boundary condition is applied to the left vertical edge. In Figure 7, the dimensionless shear stresses of the body are plotted on the elliptical contour for a cut plane placed in the middle of the longitudinal axis. The SCF value for the three-dimensional model equals to 5.7629, whereas the SCF value of the two-dimensional model equals to 5.7403, giving a deviation, i.e., a modelling error, of about 0.39%. At last, the distributions of all the components of the stress tensor are plotted in the Figure 7 showing that all the null stress components of the anti-plane shear problem disappear in the three-dimensional model as well (being of order 10^{-13}).

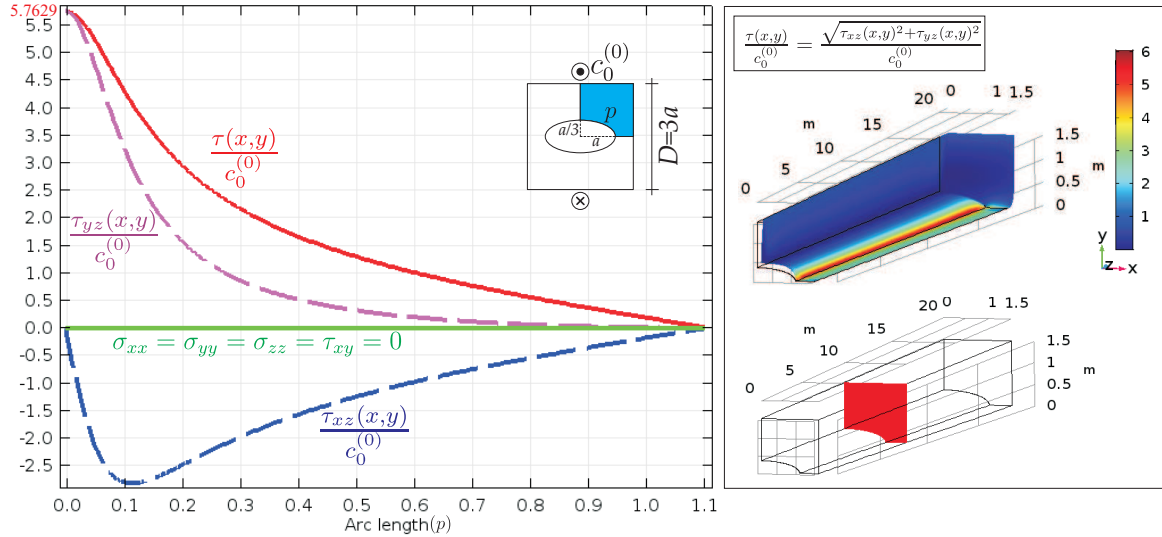


Figure 7: A quarter of a square prism with a collinear elliptical void subject to uniform anti-plane shear ($m = 0$): dimensionless shear stress field (top right), cut plane (bottom right) and dimensionless stress curves (left) on the arc length p of the elliptical contour of the cut plane.

5 Conclusions

An infinite linearly elastic plane containing an elliptical inclusion subject to an infinite class of nonuniform polynomial anti-plane shear loadings have been analyzed first analytically and then numerically. First, closed-form expressions for the complex potential and the stress concentration factor have been derived for an elliptical inclusion. The solution covers both void and rigid elliptical inclusions forming the core of the infinite plane. Second, the analytical solution in terms of stress fields has been confirmed and extended to bounded enclosures via the heat–stress analogy by using finite element analysis. A comparison between the numerical and analytical results shows that, beyond the hypothesis of an infinite plane, the analytical solution for an elliptical or a line inclusion can be used with great accuracy for the design purposes of finite planes with aspect ratios close to five. The stress intensity factor of the limiting case of an ellipse, i.e., a crack or a stiffener, have also been reported for various aspect ratios.

Acknowledgments

The authors have been supported by Academy of Finland through a project entitled Adaptive isogeometric methods for thin-walled structures (decisions 270007, 273609, 304122). The second author gratefully acknowledges the support of August-Wilhelm Scheer Visiting Professor Program established by TUM International Center and funded by German Excellence Initiative.

References

- [1] Awaja, F., Zhang, S., Tripathi, M., Nikiforov, A, Pugno, N., 2016. Cracks, micro-cracks and fracture in polymer structures: Formation, detection, autonomic repair. *Progress in Materials Science* 83, 536-573.
- [2] Bashar, M., , Sundararaj, U., Mertiny, P., 2011. Study of matrix micro-cracking in nano clay and acrylic tri-block-copolymer modified epoxy/basalt fiber-reinforced pressure-retaining structures. *eXPRESS Polymer Letters* Vol.5, No.10, 882-896.
- [3] Ahmed, M.A., Kandil,U.F., Shaker, N.O., Hashem, A.I., 2015. The overall effect of reactive rubber nanoparticles and nano clay on the mechanical properties of epoxy resin. *Journal of Radiation Research and Applied Sciences*, V. 8, Issue 4, 549-561.
- [4] Radaj, D., 1990. Design and analysis of fatigue resistant welded structures. Elsevier.
- [5] Savin, G.N., 1961. Stress concentration around holes. Pergamon Press.
- [6] Muskhelishvili, N. I., 1963. Some basic problems of the mathematical theory of elasticity. P. Noordhoff Ltd, Groningen.
- [7] Slaughter, W.S, 2002. The linearized theory of elasticity. Springer Science & Business Media.
- [8] Toubal, L., Karama, M., Lorrain, B., 2005. Stress concentration in a circular hole in composite plate. *Composite Structures*, 68, 31-36.
- [9] Givoli, D, Elishakoff, I., 1992. Stress Concentration at a nearly circular hole with uncertain irregularities. *ASME. J. Appl. Mech.* 59, 65-71.
- [10] Hoff, N.J. 1981. Stress concentrations in cylindrically orthotropic composite plates with a circular hole. *ASME. J. Appl. Mech.* 48, 563-569.
- [11] Meguid, S.A., Gong, S.X., 1993. Stress concentration around interacting circular holes: a comparison between theory and experiments. *Engineering Fracture Mechanics* 44, 247-256.
- [12] Misseroni, D., Dal Corso, F., Shahzad, S., Bigoni, D., 2014. Stress concentration near stiff inclusions: Validation of rigid inclusion model and boundary layers by means of photoelasticity. *Eng. Fract. Mech.* 121-122, 87-97.
- [13] Dal Corso, F., Bigoni, D., Noselli, G., Misseroni, D., and Shahzad, S., 2014. Rigid inclusions: stress singularity, inclusion neutrality and shear bands. *Proceedings of the 3rd International Conference on Fracture, Fatigue and Wear* p. 40-42,, Kitakyushu, Japan.
- [14] Setiawan, Y., Gan, B.S. and Han, A.L., 2017. Modeling of the ITZ zone in concrete: Experiment and numerical simulation. *Computers and Concrete*, 19, 647-655.

- [15] Zou, W.N., Lee, Y.G. and He, Q.C., 2017. Inclusions inside a bounded elastic body undergoing anti-plane shear. *Mathematics and Mechanics of Solids*, p.1081286516681195.
- [16] Shahzad, S. and Niiranen, J., 2018. Analytical solutions and stress concentration factors for annuli with inhomogeneous boundary conditions. Accepted in *ASME J Appl Mech*, doi: 10.1115/1.4040079 .
- [17] Ru, C.Q., Schiavone, P., 1997. A circular inhomogeneity with circumferentially inhomogeneous interface in anti-plane shear. *Proc. R. Soc. A* 453, 2551-2572.
- [18] Zappalorto, M., Lazzarin, P., Berto, F., 2009. Stress concentration near holes in the elastic plane subjected to antiplane deformation. *Materials Science* 48, 415-426.
- [19] Sih, G.C., 1965. Stress Distribution Near Internal Crack Tips for Longitudinal Shear Problems. *J. Appl. Mech.* 32, 51-58.
- [20] Kohno, Y., Ishikawa, H., 1995. Singularities and stress intensities at the corner point of a polygonal hole and rigid polygonal inclusion under antiplane shear. *Int. J. Eng. Sci.* 33, 1547-1560.
- [21] A. Seweryn K. Molski Elastic stress singularities and corresponding generalized stress intensity factors for angular corners under various boundary conditions. *Engineering Fracture Mechanics*, 1996; v. 55, no. 4, p. 529556.
- [22] Lubarda, V.A., 2003. Circular inclusions in anti-plane strain couple stress elasticity. *International Journal of Solids and Structures* 40, 3827-3851.
- [23] Movchan, A. B., Movchan, N. V., and Poulton, C. G., 2002. *Asymptotic Models of Fields in Dilute and Densely Packed Composites*, Imperial College Press.
- [24] Bacca, M., Dal Corso, F., Veber, D. and Bigoni, D., 2013. Anisotropic effective higher-order response of heterogeneous Cauchy elastic materials. *Mech. Res. Comm.*, 54, 63-71.
- [25] Bigoni, D., Drugan, W.J., 2007. Analytical derivation of Cosserat moduli via homogenization of heterogeneous elastic materials. *J. Appl. Mech.* 74, 1-13.
- [26] Schiavone, P., 2003. Neutrality of the elliptic inhomogeneity in the case of non-uniform loading. *Int. J. Eng. Sci.* 8, 161-169.
- [27] Van Vliet, D., Schiavone, P., Mioduchowski, A., 2003. On the Design of Neutral Elastic Inhomogeneities in the Case of Non-Uniform Loading. *Math. Mech. Solids* 41, 2081-2090.
- [28] Vasudevan, M., Schiavone, P., 2006. New results concerning the identification of neutral inhomogeneities in plane elasticity. *Arch. Mechanics* 58, 45-58.

-
- [29] Dal Corso, F., Shahzad, S., Bigoni D., 2016. Isotoxal star-shaped polygonal voids and rigid inclusions in nonuniform antiplane shear fields. Part I: Formulation and full-field solution. *Int. J. Solids Structures* 85-86, 67-75.
- [30] Dal Corso, F., Shahzad, S., Bigoni D., 2016. Isotoxal star-shaped polygonal voids and rigid inclusions in nonuniform antiplane shear fields. Part II: Singularities, annihilation and invisibility. *Int. J. Solids Structures* 85-86, 76-88.
- [31] Shahzad, S., 2016. Stress singularities, annihilations and invisibilities induced by polygonal inclusions in linear elasticity. PhD thesis, University of Trento.
- [32] Shahzad, S., Dal Corso, F., Bigoni, D., 2016. Hypocycloidal inclusions in nonuniform out-of-plane elasticity: stress singularity vs stress reduction. *Journal of Elasticity*, 126 (2), 215-229.
- [33] Chen, J., Wu, A., 2006. Null-Field approach for the multi-inclusion problem under antiplane shears. *ASME. J. Appl. Mech.* 74(3), 469-487.
- [34] Sendekyj, G. P., 1971. Multiple circular inclusion problems in longitudinal shear deformation. *J. Elast.*, 1(1), 83-86.
- [35] Gong, S. X., 1995. Antiplane interaction among multiple circular inclusions. *Mech. Res. Commun.*, 22(3), 257-262.
- [36] Lubarda, V.A., 2015. On the circumferential shear stress around circular and elliptical holes. *Arch. Appl. Mech.* 85, 223235.
- [37] Shahzad, S., Dal Corso, 2018. Torsion of elastic solids with sparsely distributed collinear voids. Under Review
- [38] Gdoutos, E.E., Rodopoulos, C.A., Yates J.R., 2003. *Problems of Fracture Mechanics and Fatigue - A Solution Guide*. Springer Science and Business Media Dordrecht.
- [39] Rice J.R., 1968. A path independent integral and the approximate analysis of strain concentration by notches and cracks. *Journal of Applied Mechanics* 35, 379-386.
- [40] Carslaw, H. S., Jaeger, J. C., 1959. *Conduction of heat in solids*. Oxford University Press.

APPENDIX - SIF for a crack in an infinite elastic plane subject to uniform anti-plane shear

We shortly give the derivation of the stress intensity factor for a crack of length $2a$ embedded in an infinite plane subject to uniform ($m = 0$) loading ($b_0^{(0)} = 0$) through equation (36). We start by exploiting the celebrated conformal mapping, $\widehat{z} = \omega(\zeta)$, and inverse mapping for a crack given as

$$\widehat{z}^{(c)} = \frac{a}{2} \left(\zeta + \frac{1}{\zeta} \right), \quad \zeta = \frac{\widehat{z}^{(c)} - \sqrt{a + \widehat{z}^{(c)}} \sqrt{\widehat{z}^{(c)} - a}}{a}. \quad (\text{I.1})$$

By using the general complex potential (22) and equations (I.1), we obtain the complex potentials in the ζ -plane and in the \hat{z} -plane as

$$g^{(c)}(\zeta) = i \frac{a c_0^{(0)}}{2} \left(\frac{1}{\zeta} - \zeta \right), \quad f^{(c)}(\hat{z}^{(c)}) = i c_0^{(0)} \sqrt{\hat{z}^{(c)} - a} \sqrt{a + \hat{z}^{(c)}}. \quad (\text{I.2})$$

The derivative of the complex potential (I.2)₂ yields the complex stress field in the physical plane as

$$\tau_{xz}^{(c)} + i \tau_{yz}^{(c)} = \frac{i c_0^{(0)} \hat{z}^{(c)}}{\sqrt{\hat{z}^{(c)} - a} \sqrt{a + \hat{z}^{(c)}}}. \quad (\text{I.3})$$

From the complex potential (I.2)₂, we obtain the displacement field as well

$$w^{(c)} = -\frac{1}{\mu} \text{Im} \left[c_0^{(0)} \sqrt{\hat{z}^{(c)} - a} \sqrt{a + \hat{z}^{(c)}} \right]. \quad (\text{I.4})$$

It should be noted that by evaluating numerically integral (36) in a counterclockwise sense, by starting along the circular contour from the lower flat crack surface $-\pi$ and continuing along the path \mathcal{C} to the upper flat surface π , one obtains the desired result. In particular, the circular contour \mathcal{C} is defined by diameter $d < 4a$ and it is centered at the crack tip with coordinates $x = a + d/2 \cos \vartheta$ and $y = d/2 \sin \vartheta$. The components of the normal vector to the circular contour are expressed by $n_x = \cos \vartheta$ and $n_y = \sin \vartheta$. The integration leads to the well-known value for the SIF

$$K_{\text{III}}^{(c)} = c_0^{(0)} \sqrt{a\pi}. \quad (\text{I.5})$$